PROGRESS IN DEVELOPING INNOVATIVE FLOW CONTROL IN A CASCADE THRUST REVERSER

Simon Hall, Emmanuel Benard, Srinivasan Raghunathan
School of Aeronautical Engineering, Queen's University Belfast, UK

Keywords: *Thrust Reverser, Flow Control*

Abstract

Aircraft thrust reverser design can be potentially improved by replacement of mechanical flow control devices with fluidic flow control. An experimental and computational program to analyse flow in a natural blockage type reverser duct has been undertaken and has identified the delay of inlet ramp flow separation and reduction of flow blockage as being objectives for the application of flow control.

1 Introduction

Almost all modern jet transport aircraft have engine nacelles incorporating a thrust reversal system. The system is activated during the aircraft ground roll and blocks the core and/or fan duct of the nacelle redirecting the flow outwards and forwards to produce a braking thrust force. Primarily installed as a safety feature the thrust reverser is used to augment deceleration in adverse weather conditions when mechanical brake performance is degraded or when additional braking is required during abortive take off situations. However the system is also used in daily operations to reduce mechanical brake wear and to expedite runway egress.

Some types of thrust reverser redirect both the core and fan flow post-exit of the nacelle however the majority of reversing systems operate pre-exit on the fan flow only. The most common type of fan flow thrust reverser consists of a transcowl, cascade and blocker door. When the system is activated the transcowl moves aft to expose the cascade whilst the blocker door pivots to block the fan duct. The blocker door deflects the fan flow outwards through the transcowl opening and the cascade turns the flow forwards to produce the reverse thrust force. Other forms of thrust reverser are the pivoting door type reverser and the natural blockage type reverser. The pivoting door type reverser uses the inner surface of the blocker door along with a kicker plate to redirect the flow forwards in place of a cascade. The natural blockage type reverser, which is the type forming the basis for this research uses an S-shaped fan duct so that the transcowl blocks the duct when it translates aft obviating the need for a blocker door. Fig 1 shows a typical natural blockage cascade type thrust reverser in stowed and deployed state.

In general the thrust reverser system is complex and represents a considerable part of the overall nacelle weight, as much as 30% for a large bypass ratio turbofan. In addition it is a major source of noise during landing and increases aircraft specific fuel consumption through transcowl leakage during cruise. It is the goal of the thrust reverser designer to achieve maximum reverse thrust performance whilst minimizing nacelle pressure losses (leakage) and system weight. Lord et al [1] have suggested the use of fluidic flow control as an alternative to the mechanical blocker door and/or cascade system. The lack of mechanical control devices could reduce the weight of the system and also reduce the pressure leakage by having fewer nacelle gaps. This paper presents results of an ongoing research project to investigate the aerodynamics of several thrust reverser concepts incorporating fluidic flow control. Specifically the objectives of the research project are to computationally and experimentally test possible fluidic flow control configurations in a generic thrust reverser duct model and to compare the fluid dynamics and performance of these configurations with a conventional cascade arrangement. It is hoped that the results of the project will go some way to proving that fluidic flow control is a viable alternative to existing mechanical flow control devices in thrust reversers. The results presented in this paper describe the initial testing of the duct model without fluidic flow control. When the cascade is fitted to the model the cascade geometry is expressed in terms of the ratio of the cascade vane chord *(c)* to horizontal vane spacing *(s)*. Three configurations are tested: *c/s = 1.56*, *c/s = 1.13* and *c/s = 0* i.e. no cascade fitted. The paper describes the analysis tools for the research and highlights some important flow control issues that will need to be subsequently addressed.

2 Methodology

The thrust reverser model is a 50% scale 2D representation of a generic S-shaped fan duct as found in a natural blockage type thrust reverser. The aspect ratio of the rectangular duct cross-section is 4.2 and the inlet cross-section of the model measures 380x90mm. The experimental model is tested on a low speed wind tunnel with maximum inlet velocity of approximately 15m/s. For conventional thrust reverser configurations Poland [2] has confirmed experimentally that model scale effects do not significantly affect performance estimation whilst Yao et al [3] concluded that low Mach number/low Reynolds number experiments are adequate to investigate higher Mach number/Reynolds number flow fields in a conventional natural blockage type thrust reverser.

In the experimental model static pressure tappings are mounted in the upper and lower duct surfaces on the model centerline and also in the spanwise direction at a mid-duct position on the lower surface. An internal traversing total pressure rake and static pressure tappings at the model inlet record the inlet flow pressure. Fig 2 shows the model geometry along with the locations of the surface static pressure tappings.

The pressure data recorded during the experimental and computational tests is presented in terms of pressure coefficient:-

$$C_p = \frac{P - P_a}{\frac{1}{2}\rho U_{ref}^2} \tag{1}$$

Where P_a is the atmospheric pressure datum and U_{ref} is a notional isentropic propulsive nozzle velocity. This is obtained from an assumed isentropic expansion through the nozzle. Based on this assumption U_{ref} =1.76 U_m where U_m is the measured mean inlet velocity.

The surface static pressure coefficients are given at positions along the bottom wall corresponding to the horizontal distance relative to the inlet plane (*X*). There is a problem with the same scheme for the upper wall since at the inlet ramp the wall doubles back on itself. Therefore for the upper surface case the positions are presented in terms of a modified horizontal distance (*modX*). The apex of the inlet ramp on the upper surface is defined as X_{max} = *0.263m*. The modified horizontal distance is expressed as the apex distance plus the modulus of the distance from the apex to the post-apex position in question.

The model was also analysed computationally using the commercial CFD package FLUENT 6™. The CFD model was two-dimensional rather than three-dimensional to reduce computation time and cost. The CFD analyses used the Reynolds Averaged Navier-Stokes (RANS) viscous flow equations. The flow was assumed to be steady and incompressible and so the segregated implicit flow solver was used. The flow domain was discretised using an unstructured mesh with 29143 nodes.

Previous attempts to numerically simulate flow in complex internal ducts have met with problems regarding turbulence modelling. Kral [4] notes that the presence of large scale secondary flow structures and separated flow regions within complex internal ducts places a high demand on the turbulence model.

A number of turbulence models were tested for the case *c/s = 1.56*. Figure 3 shows the results of these tests alongside experimental data for the same flow conditions. Note the wide discrepancy in numerical values. The standard K-ε turbulence model appears to give results which best compare with the experimental data and this turbulence model was used for the remainder of the CFD analyses.

The boundary layer flow close to the model walls and cascade vanes was modelled using wall functions with wall adjacent cells having cell height in terms of wall units of $y^+ \approx 20$. To ascertain the accuracy of these wall functions a simulation was performed with the domain discretised with 534938 nodes with the boundary layer resolved down to the viscous sublayer (wall adjacent cells $y^+<1$). Figure 4 shows the static pressure coefficient computed on the lower duct surface for the two meshes in comparison with the experimental results for the same flow conditions. The thick line appearance of the fine mesh result is in fact small scale fluctuations in the pressure which do not show up clearly due to the figure resolution. The variation between the results appears small and both CFD models capture the shape of the experimental data very well at least up to the separated flow region at $X \approx 300$ *mm*. Varying the mesh size also resulted in a variation in mass flow rate at the cascade exit of less than 2%.

It should be noted that a large degree of the error in the CFD results may be due to the two-dimensional nature of the models. Flow visualization performed during the experiments confirmed the presence of corner vortices on the lower duct surface and sidewalls and such flow structures are not captured by the 2D CFD model.

3 Results and Discussion

Results are presented showing the internal surface static pressure coefficient distribution on the model centerline for *c/s = 1.56*, *c/s = 1.13* and *c/s = 0*. These three cases have respective mean inlet velocities of *13.48m/s, 14.33m/s* and *14.79m/s*.

Figures 5 and 6 show the static pressure coefficient distributions on the duct surfaces for the various configurations. Looking first at the experimental results, the initial drop in pressure coefficient on the lower surface suggests that the flow here is accelerating as it moves along the straight duct section after the initial 30^0 duct bend. The simultaneous increase in pressure coefficient on the upper surface indicates the flow decelerating here as it moves along the straight duct section. As the flow passes through the initial duct bend it experiences a radial pressure gradient corresponding to centrifugal pressure. Close to the duct sidewalls the flow experiences less pressure gradient since it is almost at rest. This causes the flow to move radially outwards to a greater degree in the centre of the duct cross-section and subsequently sets up a double circulation in the cross-section which when combined with the primary flow forms into two corner vortices on the lower surface. The presence of such vortices was confirmed in flow visualization tests using china clay. In the flow visualization tests it was noted that the vortices first appeared at the end of the initial duct bend and developed in size downstream in the straight duct section. The transportation of fluid away from the upper surface towards the lower surface by the secondary flow in the straight duct section could explain the flow velocity increase on the lower surface and velocity decrease on the upper surface. As the inlet ramp is approached the pressure coefficient on the upper surface drops sharply indicating a rapid acceleration of the flow around the inlet ramp corner. On the lower surface normal to the beginning of the inlet ramp the pressure coefficient rises as the flow slows down. The straight duct approach to the inlet ramp appears to follow the classical behaviour of duct flow preceding a bend with the upper surface experiencing a favourable pressure gradient and the lower surface experiencing an adverse pressure gradient. The favourable pressure gradient on the upper surface causes the flow to accelerate here whilst on the lower surface the adverse pressure gradient acts against the corner vortices to reduce the acceleration rate along this surface.

Prior to the apex of the inlet ramp the upper surface pressure coefficient levels off suddenly indicating a flow separation. Similarly on the lower surface a plateau in the static pressure coefficient at $X \approx 320mm$ suggests a separation of flow on this surface also. The flow around the inlet ramp creates a severe adverse pressure gradient which causes the separation on the lower surface. Similarly as the flow turns around the inlet ramp surface the change in cross-sectional area causes a rapid expansion of the flow which leads to the separation from the inlet ramp itself. These features are confirmed by the surface flow visualization.

For increases in *c/s* the overall static pressure coefficient levels rise throughout the duct. There is little change in the shape of the pressure coefficient distribution along both surfaces although on the upper surface it appears that for the cascade installed cases (*c/s=1.13* & *c/s = 1.56*) the inlet ramp separation occurs later than for the case with no cascade. It is the authors' belief that the ability of the reverser and cascade to deflect the flow forwards hinges on delaying the separation from the inlet ramp. Comparing the CFD predicted pressure coefficients with the experimental results in figures 5 and 6 the accuracy of the results for the *c/s = 1.56* case appears fortuitous and is not repeated for the other cases. Despite using the same K-ε turbulence model and boundary mesh the results for the other two cases are not as close a match to their respective experimental results. This emphasises the difficulty in obtaining a CFD model which gives quantitative accuracy across all cascade geometry test cases. Due to both the complex geometry and flow phenomena computational modeling of internal thrust reverser flow remains a challenge.

None of the CFD solutions accurately capture the flow separation on the upper and lower surfaces. In particular in figure 5 the CFD results show no flow separation prior to the inlet ramp apex on the upper surface. The surface flow visualization tests on the *c/s = 1.13* configuration confirmed that flow separation occurred prior to the inlet ramp apex at a position of *ModX = 260mm*. Flow separation was also observed on the lower surface at position *X = 306mm*. The presence of three-dimensional flow structures in the duct may go some way to explaining the failure of the CFD to accurately capture the flow separation. The two-dimensional nature of the CFD model means that 3D flow structures cannot be captured. It is speculated that the secondary flow structures in the real flow lead to a reduction in the ability of the flow to turn. This would have the effect of reducing the turning efficiency of the geometry and would lead to a larger pressure difference (higher *Cp*) being required to maintain the mass flow rate through the duct. Despite the problems already identified 2D CFD modeling is still useful for qualitative analysis. Referring again to figures 5 and 6 note that the CFD results do record the occurrence of a flow separation on both surfaces. They also accurately record the shape of the pressure distribution on the surfaces up to the region of separation as well as the fact that the overall pressure coefficients increase with increased *c/s*. An advantage of the 2D CFD modeling is the fact that results can be produced relatively rapidly. The cases published here reached converged solutions in 2 hours running on a relatively standard PC (Intel Pentium 4, 2.4 GHz processor).

From the CFD analyses the mass flow rate is calculated at the reverser duct exit for each configuration. The results are displayed in table 1.

Table 1. Mass flow rate at duct exit

c/s ratio	Exit mass flow rate (kg/s)
0.00	1.720
1.13	1.036
1.56	0.707

It is clear that the increase in static pressure coefficients for increasing *c/s* ratio correlates with a decrease in mass flow rate at the duct exit. The flowfield streamlines generated by the CFD analyses provide a very useful tool for helping to explain variations in data such as this. Figures 7-9 show the streamline plots for the 3 cases in the region of the duct exit. For the *c/s = 0.0* case the flow exits with very little forward deflection. For *c/s = 1.13* the presence of the cascade produces a much greater deflection of the flow. For *c/s = 1.56* there is another but smaller increase in flow deflection. The presence of an increasing number of cascade vanes at the duct exit will naturally reduce the exit area through which the flow can pass. Similarly increasing the degree of flow deflection will cause a reduction in effective exit area. In previous experiments Romine and Johnson [5] noted that losses in the thrust reverser are a function of the cascade effective area. As deflection angle increases the cascade effective area decreases leading to increased flow blockage and a drop in flow discharge. The results from the analyses here appear to tie in with this statement. Increasing the *c/s* ratio leads to increased flow deflection but also increases the flow blockage leading to reduced mass flow rate at the exit and higher static pressure levels inside the duct.

4 Conclusions and Next Actions

This paper details what are essentially the first stages in the program to research fluidic flow control in a thrust reverser. The results suggest that the key to creating efficient flow deflection in the reverser lies in the shape of the inlet ramp surface and preventing flow separation from this surface. In addition, improved duct efficiency might be achieved by reducing flow blockage. The next stage in the project is to implement fluidic flow control in the form of tangential wall jets, which will be tested on both the inlet ramp surface and blocker wall surface in various configurations. The design aim will be to determine if separation on the inlet ramp can be delayed or can be achieved at similar levels to the cascade but with reduced flow blockage i.e. higher efficiency.

The experimental model is currently being reconfigured for these tests which will be conducted on a more powerful wind tunnel with a maximum inlet velocity of 40m/s. A 3-component force balance is being installed to allow direct force measurements on the model, which will provide a performance evaluation metric. Provision is also being made for PIV measurements at a later date.

On the computational side 3D mesh simulations are in progress. It is hoped that these CFD simulations will allow further insight into the structure and extent of the 3D effects in the flow. However owing to the computation times involved the majority of qualitative flow tests will still be carried out using the 2D meshes.

References

[1] Lord W K, MacMartin P G and Tillman T G. Flow control opportunities in gas turbine engines. AIAA 2000-2234, 2000.

[2] Poland D T. The aerodynamics of thrust reversers for high bypass turbofans. AIAA 67-418, July 1967.

[3] Yao H, Benard E, Cooper R K, Raghunathan S, Tweedie J and Riordan D. Aerodynamics of natural blockage thrust reverser. *Proceedings of CASI 50th AGM & Conference, April 28-30 Montreal, QC.* Paper 329, 2003.

[4] Kral, L D. Recent experience with different turbulence models applied to the calculation of flow over aircraft components. *Progress in Aerospace Sciences,* Vol 34, pp 481-541, 1998.

[5] Romine Jr B M and Johnson W A. Performance investigation of a fan thrust reverser for a high bypass turbofan engine. AIAA-84-1178, *AIAA/SAE/ASME 20th Joint Propulsion Conference, Cincinnati, USA.* June 1984.

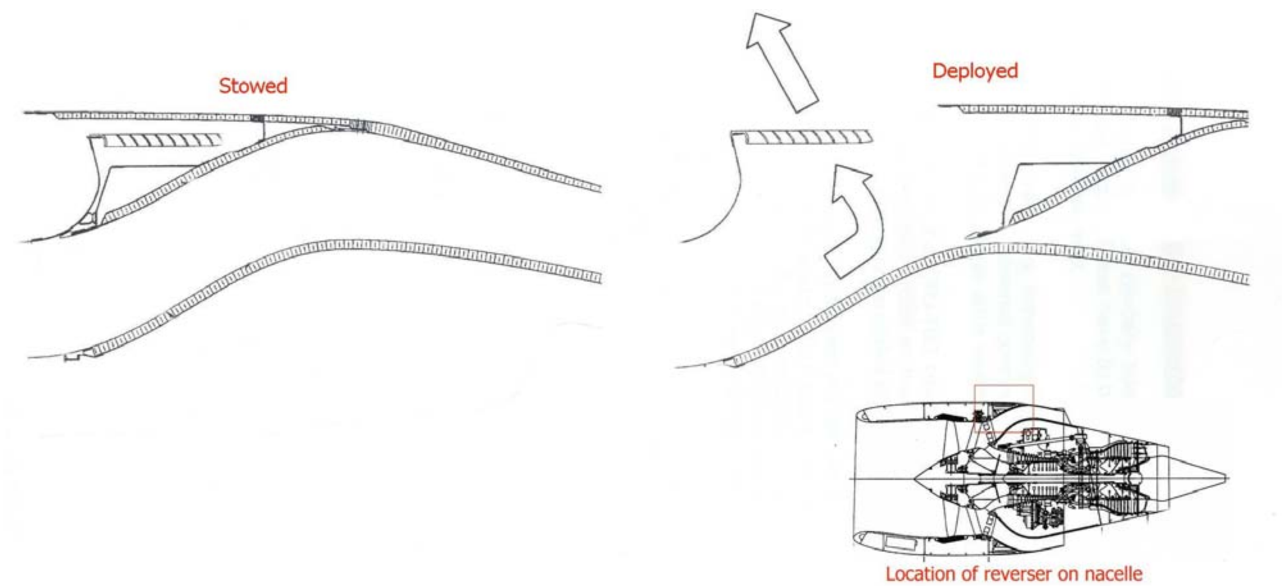

Fig 1. General arrangement of natural blockage type thrust reverser.

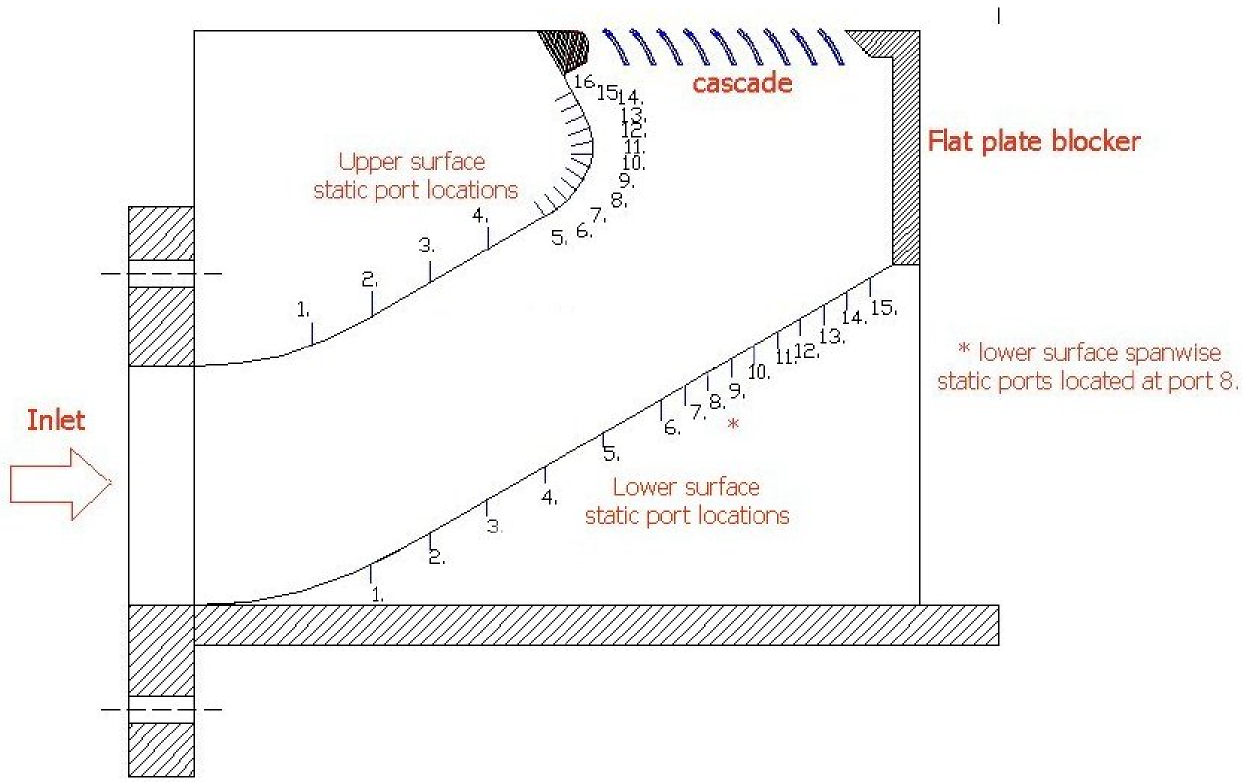

Fig 2. Model duct geometry.

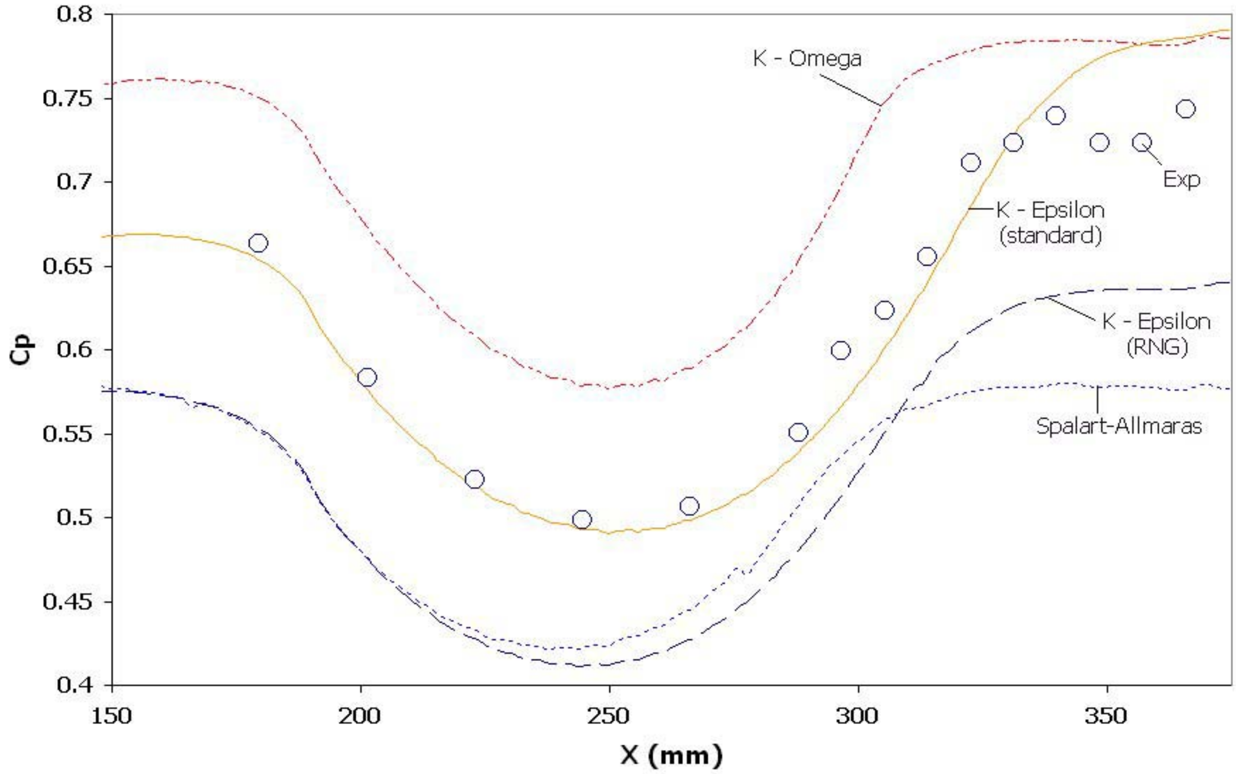

Fig 3. Static pressure coefficient distribution on lower internal surface for configuration *c/s = 1.56*.

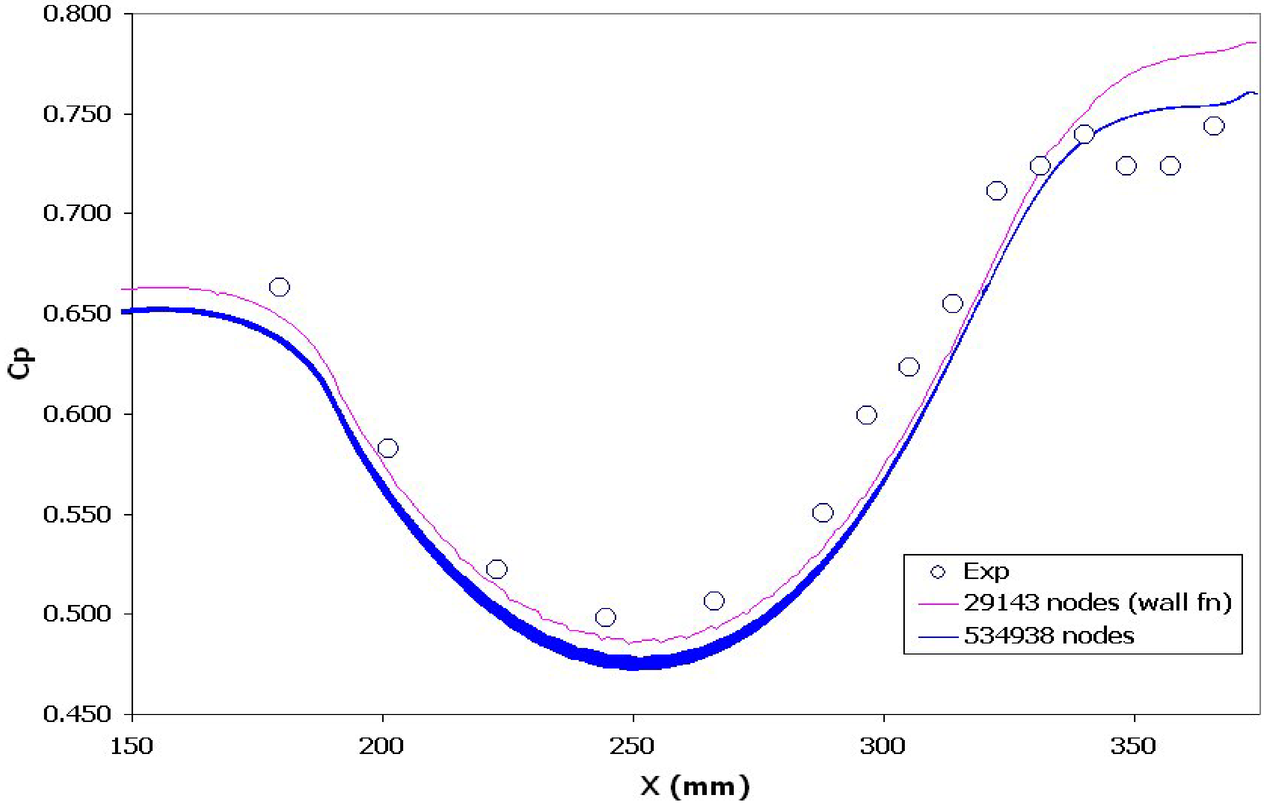

Fig 4. Static pressure coefficient distribution on lower internal surface for configuration *c/s = 1.56*.

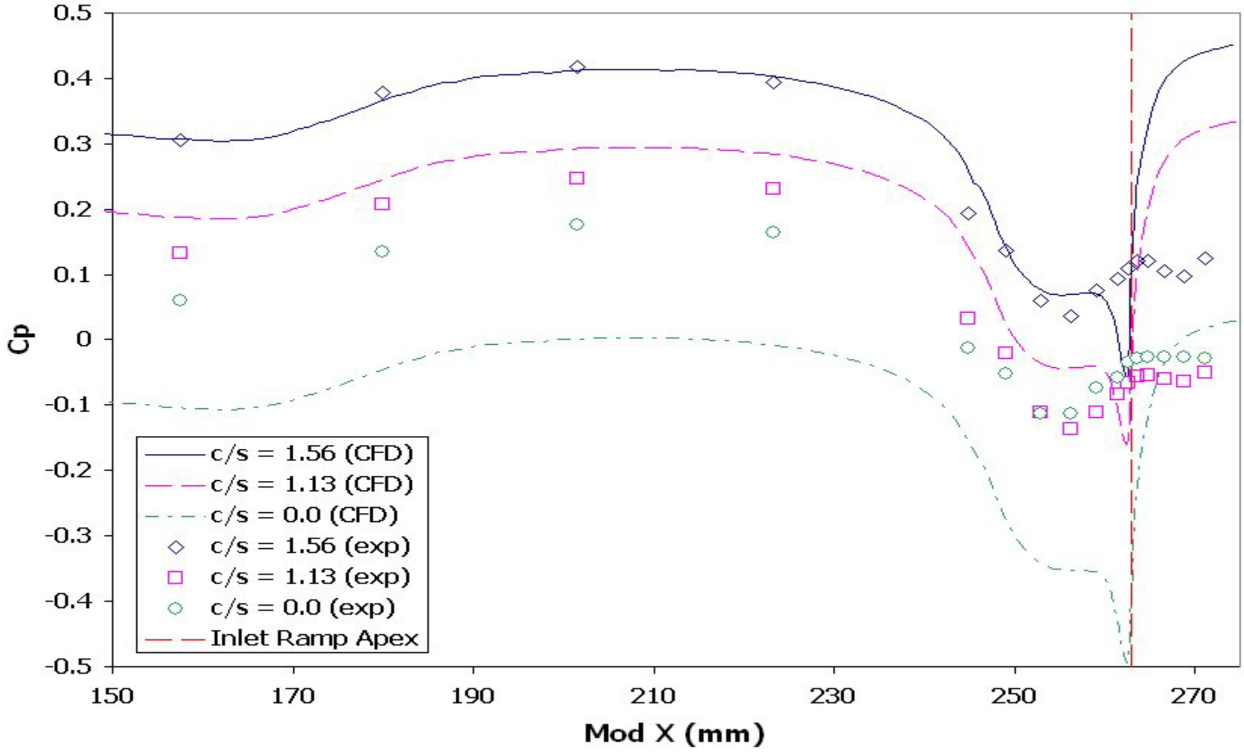

Fig 5. Experimental static pressure coefficient on upper internal surface.

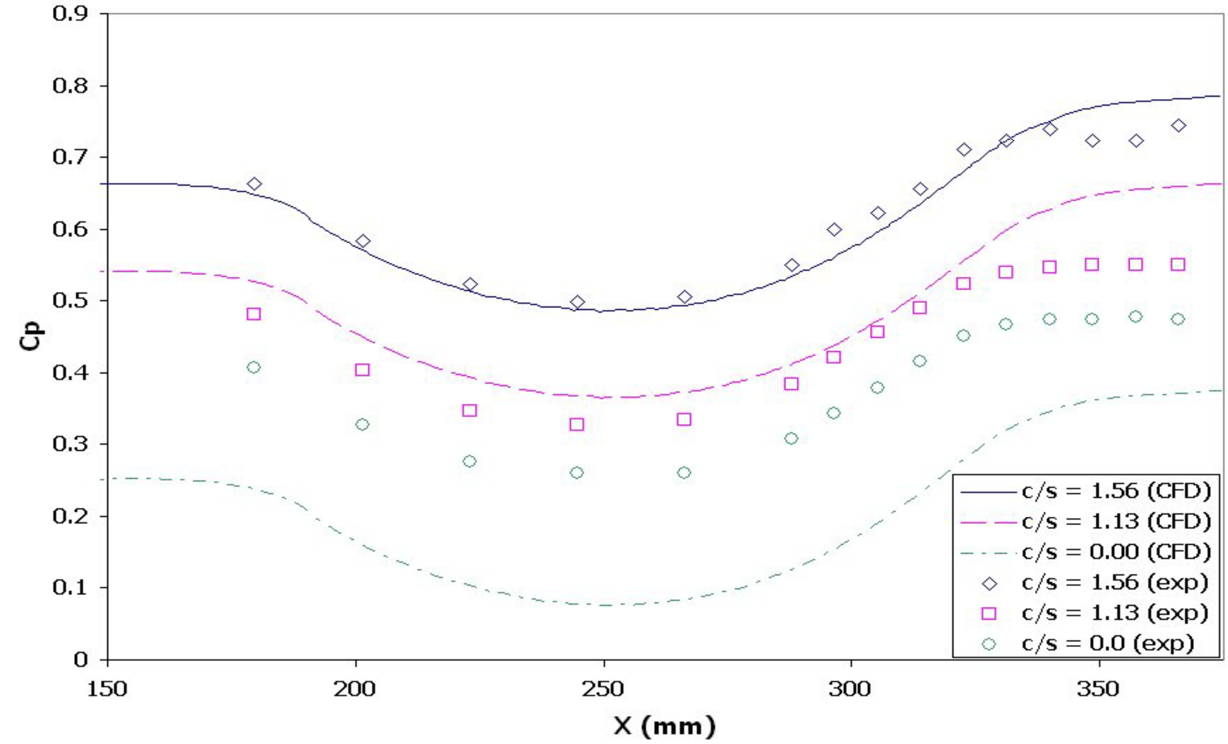

Fig 6. Experimental static pressure coefficient on lower internal surface.

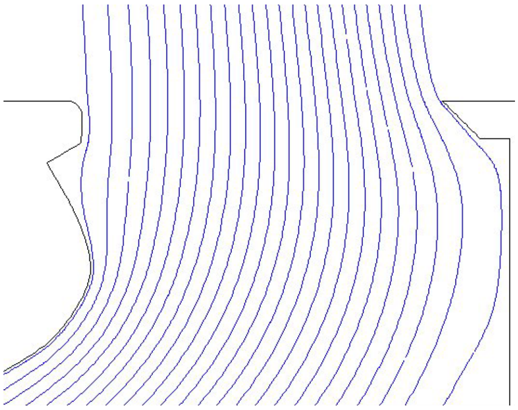

Fig 7. Streamline plot at duct exit c/s = 0.00.

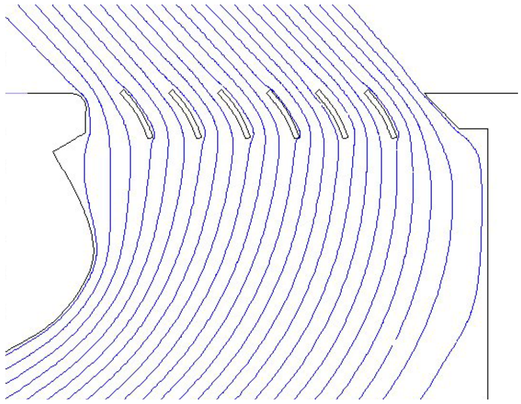

Fig 8. Streamline plot at duct exit c/s = 1.13.

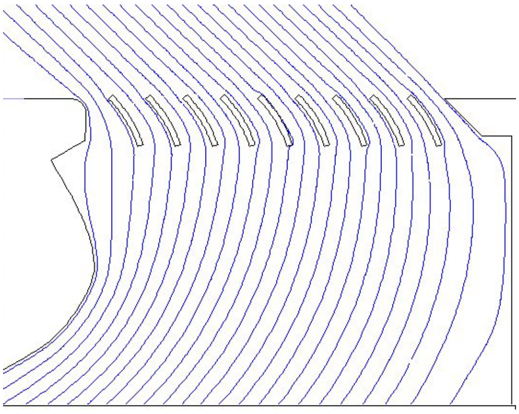

Fig 9. Streamline plot at duct exit c/s = 1.56.